Modulating Iron Spin States with Radical Ligands: A Density Functional Theoretical Study

*Ludovica Credendino and Stephen Sproules**

[*] L. Credendino, Dr. S. Sproules
WestCHEM School of Chemistry, University of Glasgow
Glasgow G12 8QQ (UK)
Email: stephen.sproules@glasgow.ac.uk

Dedicated to Professor Karl Wieghardt on the occasion of his 95th birthday

Supporting Information. Optimized metric parameters and population analyses for all complexes; qualitative MO schemes and spin density plots. Supporting information for this article is available on the WWW under https://doi.org/10.1002/ajoc.2020XXXXX

Abstract. The ground state electronic structures of $[Fe^{III}X(L^{ISQ})_2]^0$ where X is a halide (F^-, Cl^-, Br^-, I^-) or pseudo-halide (N_3^-, NCS^-) and $(L^{ISQ})^{1-}$ is the *o*-iminobenzosemiquinonato π-radical ligand, have been calculated using DFT at the B3LYP* level of theory. The modified functional with 15% Hartree-Fock exchange is required to successfully reproduce the spin ground state of the complex as either $S = {}^3/_2$ for X = F^-, Cl^- and NCS^-, or $S = {}^1/_2$ for X = Br^-, I^- and N_3^-. The difference in ground state stems from an $S_{Fe} = {}^5/_2 \rightarrow S_{Fe} = {}^3/_2$ spin transition at the iron ion, prompted by the donor properties of the apical ligand. The computational methodology was validated through accurate calculation of the Mössbauer parameters. The redox chemistry of the *o*-aminophenolate ligand was examined for the putative five-membered electron transfer series for $[Fe^{III}F(L^{ISQ})_2]^z$ and $[Fe^{III}I(L^{ISQ})_2]^z$ (z = 2+ 1+, 0, 1–, 2–). The redox chemistry is entirely ligand-centered with retention of the ferric ion, where only the strong ligand field provided by a fully reduced *o*-anilinophenolate(2–) ligand in conjunction with a soft apical donor will support an intermediate-spin Fe(III) central ion.

Introduction

Transition metal compounds that catalyze C–C coupling and C–H activation reactions traditionally involve elements from the platinum group.[1] This collection of six metals – ruthenium, rhodium, palladium, osmium, iridium and platinum – are described as “noble” on account of their resistance to corrosion, and precious given their low terrestrial abundance that confers high economic value. Costs aside, the success of the platinum group resides with their intrinsic ability to perform two-electron chemistry, while tolerating a wide range of substrates, functional groups and reaction conditions. With the advent of green chemistry and the promotion of sustainability, there is growing interest in using more Earth abundant elements, the base metals from the first row of the d-block.[2,3] The challenge of these metals is to simultaneously suppress their tendency for one-electron chemistry and promote two-electron reactivity akin to the platinum group. This so-called base metal ennoblement is achieved by partnering the base metal with a redox-active ligand.[4]

Over the last decade, this method has prospered in large part from the ability to tune the redox-interplay between the base metal and ligand components.[2,5] Our understanding of coordination complexes with redox-active ligands stems from a series of fundamental studies inspired by the operation of certain metalloenzymes, in particular *galactose oxidase* – a copper protein with a radical tyrosinyl ligand that performs the two-electron oxidation of alcohols to aldehydes.[6] Although redox-active ligands had been known for some time, our ability to define their electronic structure by unambiguously determining their oxidation level remand largely out of reach until the arrival of high resolution X-ray crystallography which gave very precise intraligand bond distances.[7,8] Access to new methods, such as X-ray spectroscopy which utilizes synchrotron radiation presented the option to selectively probe individual redox-active centers in a complex.[9,10] At the forefront of this redox redux was the Wieghardt group at the MPI for Bioanorganische Chemie who applied an arsenal of physical methods to unambiguously diagnose the electronic structures of a swathe of compounds with an assortment of redox-active ligands.[7,8] Chief among these were *o*-aryl chelates with *N*,*N*′ (diimine) *O*,*O*′ (dioxolene) *O*,*N* (aminophenol) *N*,*S* (aminothiophenol) *S*,*S*′ (dithiolene) donor atoms whose redox chemistry is instigated via coordination to a transition metal ion (Figure 1).[10,11] Many of the

compounds investigated contained a central iron ion with one, two or three of these redox-active chelates as their electronic structures can be challenging to define, and so there existed several unsubstantiated assignments that were either confirmed or reevaluated. One notable example was the report of [Fe^{IV}('N_2S_2')(P^nPr_3)] and [Fe^{V}('N_2S_2')I], where 'N_2S_2' is tetradentate 1,2-ethanediamine-*N*,*N*′-(2-benzenethiol).[12] These compounds were originally defined as possessing high-valent Fe(IV) and Fe(V) ions, respectively, which according to ligand field theory seemed improbable. A subsequent experimental and computational reexamination gave the electronic structure as a central intermediate-spin Fe(III) S_{Fe} = $^3/_2$ ion with a one- and two-electron-oxidized 'N_2S_2' radical ligand.[13] Hence, it is vital to accurately define the electronic structures in order to predict the reactivity and utility of a particular combination of metal ion and redox-active ligand, as still to this day spurious assignments continue to be reported.[14]

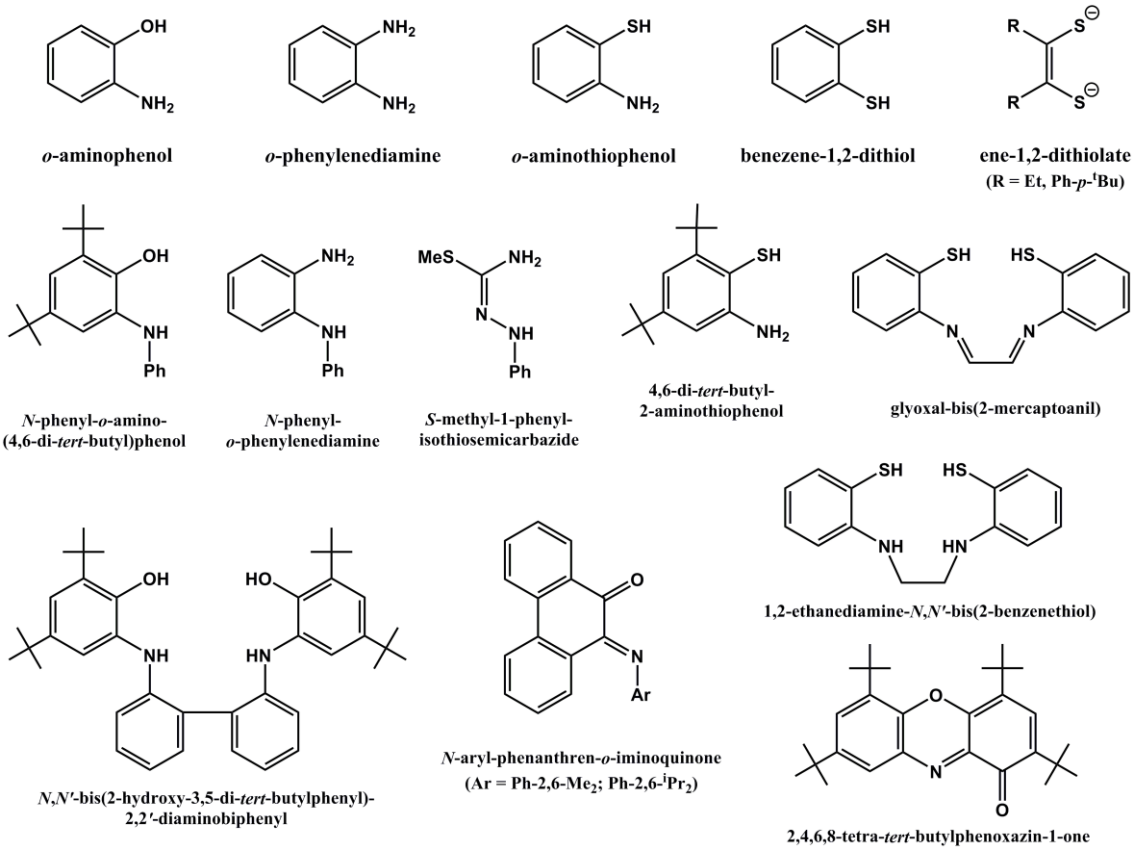

Figure 1. Catalogue of *O*,*N*-, *N*,*N*′-, *N*,*S*- and *S*,*S*′-donor chelating ligands that give [$Fe^{III}X(L)_n$] (X = halide or pseudo-halide; *n* = 1 or 2) complexes.

Five-coordinate, square pyramidal iron compounds with the formula [$Fe^{III}X(L)_n$] (X = halide or pseudo-halide; n = 1 or 2), where L is a bidentate or a tetradentate redox-active ligand, are archetypal examples where the ligand field supports an intermediate-spin iron ion (Figure 1).[13,15-19] Many of these compounds were the subject of detailed electronic structure studies that produced a blueprint for the establishing oxidation levels for the redox centers, and these where often augmented by computational studies that were among the first to apply the broken-symmetry (BS) formalism to monometallic systems.[11,14,16,19-22] However, five-coordinate iron complexes with chelating *o*-aminophenols have as yet not been examined computationally because they exhibit a unique $S_{Fe} = {}^3/_2 \rightarrow S_{Fe} = {}^5/_2$ spin transition at an experimentally observable temperature.[17,18] The two redox-active chelates are at the *o*-iminobenzosemiquinato $(L^{ISQ})^{1-}$ oxidation level irrespective on the iron spin state (Scheme 1). The spin transition is dictated by the nature of the apical ligand, such that [FeI(L^{ISQ})$_2$] has an $S = {}^1/_2$ spin ground state up to room temperature whereas [FeCl(L^{ISQ})$_2$] is $S = {}^3/_2$.[18] Magnetic susceptibility and Mössbauer measurements reveal that a sample of [FeBr(L^{ISQ})$_2$] is $S = {}^1/_2$ up to 140 K, where upon the spin transition occurs producing a proportion of the sample with $S = {}^3/_2$ spin state.[17] A second polymorph of [FeBr(L^{ISQ})$_2$] was isolated and shown to be $S = {}^3/_2$ for the full temperature range. Moreover, two complexes with pseudo-halide *N*-donor azido and isothiocyanate ligands, [Fe(N_3)(L^{ISQ})$_2$] and [Fe(NCS)(L^{ISQ})$_2$], have $S = {}^1/_2$ and $S = {}^3/_2$ spin ground states, respectively.[17] Herein we present a DFT analysis of the electronic structures of these five-coordinate iron compounds, and use the experimental data to calibrate our DFT protocol. The [FeF(L^{ISQ})$_2$] complex is included to complete the series for all halide ligands and to compare with the other 2p ligands N_3^- and NCS^-. The veracity of the computational method is tested in the reproduction of structural metrics and calculated Mössbauer parameters, as well as comparing the energy for the $S = {}^1/_2$ and the $S = {}^3/_2$ ground states. We further investigate the redox chemistry of these complexes by predicting both the iron and total spin ground state for the five-membered series from dication to dianion, which are interrelated by one-electron transfer processes localized to the *o*-aminophenolate ligand. This study is timely considering that *o*-aminophenolate ligands have already been employed in a range of chemical transformations utilizing Fe,[23] Co,[24] and the somewhat less abundant Re.[25] The

results presented here highlight not only the importance of ligand-based redox chemistry on the utility of Earth abundant metals in catalysis but also the effect of modifying the ligand field has on the spin state and therein reactivity of the central iron ion.

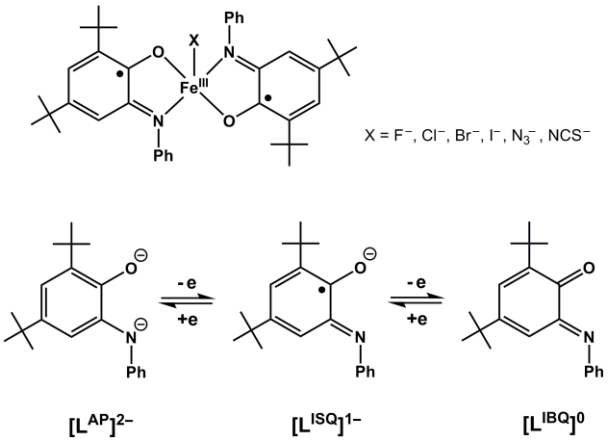

Scheme 1. Structure of the $[Fe^{III}X(L^{ISQ})_2]^0$ (X = F^-, Cl^-, Br^-, I^-, N_3^-, NCS^-) compounds under study, and the three oxidation levels (charge state) of the *O,N*-coordinating *o*-anilinophenolate dianion, $(L^{AP})^{2-}$, *o*-iminobenzosemiquinonate anion, $(L^{ISQ})^{1-}$, and neutral *o*-iminobenzoquinone ligand, $(L^{IBQ})^0$.

Results and Discussion

1. Ligands. The geometry for each ligand oxidation level was optimized at the BP86/def2-TZVPP level of theory. Calculations were performed on charge-neutral species where the different oxidation levels were accessed by varying the protonation: the parent 2-anilino-4,6-di-*tert*-butylphenol, $H_2[L^{AP}]$, its one-electron oxidized form, $H[L^{ISQ}]$, and the fully deprotonated two-electron oxidized form *o*-iminobenzoquinone, $[L^{IBQ}]$ (Scheme 1). The optimized bond distances for the fully protonated *o*-anilinophenol molecule closely match the experimental values (Table 1).[7] The characteristic structural trends are observed for successive removal of electrons from the π-system. Given the asymmetry of the donor atoms, the first oxidation giving the *o*-iminobenzosemiquinonato(1–) radical impacts the amine group with pronounced shortening of the two N–C bonds compared with the fully reduced form. The O–C bond is largely unchanged. The formation of a benzosemiquinone results in the hallmark four-long/two-short C–C distances of the ring giving a long average aromatic C–C bond length of

1.422 Å. These computed distances are in good agreement with experimental values for other complexes with L^{ISQ} radicals.[26] The magnitude of the quinoidal distortion, being greater than the 3σ confidence interval, is reflected in the spin density distribution for the L^{ISQ} radical where half the spin is delocalized over the aromatic ring in an alternating spin-up/spin-down pattern (Figure 2). The largest concentration is found on the imino group, identified as the locus of one-electron oxidation. Further oxidation to the iminobenzoquinone results in substantial shortening of the O–C distance commensurate with a bond order of 2. The quinoidal distortion increases as measured by the average aromatic C–C bond length of 1.446 Å. This trend is borne out experimentally when compared to the structural parameters obtained for *p*-trifluoromethylphenyl iminobenzoquinone.[27]

Table 1. Calculated interatomic distances (Å) for the three ligand oxidation levels.[a]

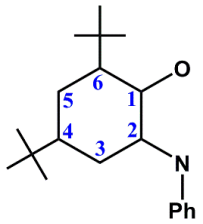

	$H_2[L^{AP}]$ [b]		$H[L^{ISQ}]$ [c]		$[L^{IBQ}]$ [d]	
O–C1	1.360	(1.376(3))	1.355	(1.299(4))	1.234	(1.214(1))
N–C2	1.437	(1.431(4))	1.350	(1.350(4))	1.304	(1.286(1))
N–C_{Ph}	1.414	(1.409(3))	1.373		1.387	(1.406(1))
C1–C2	1.413	(1.388(4))	1.457	(1.445(5))	1.536	(1.524(1))
C1–C6	1.421	(1.404(4))	1.421	(1.434(4))	1.486	(1.480(1))
C2–C3	1.402	(1.394(4))	1.436	(1.416(5))	1.453	(1.450(1))
C3–C4	1.404	(1.386(4))	1.386	(1.365(5))	1.369	(1.345(1))
C4–C5	1.415	(1.401(4))	1.425	(1.442(5))	1.462	(1.466(1))
C5–C6	1.406	(1.392(4))	1.404	(1.380(5))	1.372	(1.347(1))
avg. C–C	1.411	(1.395(4))	1.422	(1.414(5))	1.446	(1.435(2))

[a] From BP86/def2-TZVPP calculations; [b] Experimental data in parentheses taken from ref. [7]; [c] Experimental data in parentheses taken from ref. [26]; [d] Experimental data in parentheses taken from ref. [27].

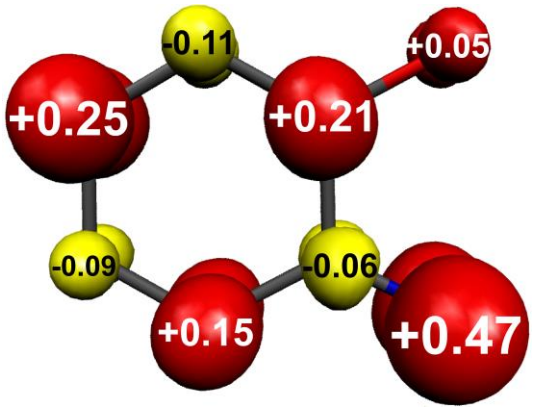

Figure 2. Mulliken spin population analysis for the H[L^{ISQ}] radical.

2. Neutral complexes. The halide and pseudo-halide complexes in this series, [FeX(L^{ISQ})$_2$], were also optimized using the BP86/def2-TZVPP protocol. For X = Cl, Br, I, N_3 and NCS, crystallographic coordinates provided the starting point for the optimization.[17,18] In lieu of crystal structure for [FeF(L^{ISQ})$_2$], the isothiocyanate complex was modified by replacing the apical donor with a fluorine atom. For each compound, the spin-quartet (S = $^3/_2$) and spin-doublet (S = $^1/_2$) geometries were computed. The salient metrics for all complexes are compiled in Table 2 and show very good agreement with the experimental data. Instances where the experimental and calculated bond distances diverge is due to the presence of both S = $^3/_2$ and S = $^1/_2$ forms in some of these compounds at the temperature which diffraction data were collected.[17] Intraligand bond distances match those calculated for the L^{ISQ} oxidation level such that each complex has a ferric ion coordinated by two π-radical anions (S_L = 1). The total spin ground state is either S = $^3/_2$ when the central Fe(III) ion is high-spin (S_{Fe} = $^5/_2$) or S = $^1/_2$ when the Fe(III) ion is intermediate-spin (S_{Fe} = $^3/_2$).

The effect of the Fe spin state on the π-radical ligands is minimal, as evidenced by the calculated average aromatic C–C bond distance of ~1.424 Å for the S = $^3/_2$ molecules being only slightly longer than the ~1.419 Å distance in the S = $^1/_2$ species (Tables S1 and S2). Across the series, the O–C bond in the spin-quartet species is 0.02 Å shorter than the same bond in the spin-doublet complexes (Tables S1 and S2). This trend is also observed for the N–C bond distance, and reflects the different orbital population associated with the spin transition that is centered on the d-orbitals orthogonal to the

Fe–X unit. As such, the Fe–X distance remains the unchanged irrespective of the spin state at Fe, as was shown with the two crystal structures of [FeBr(L^{ISQ})$_2$] with S = $^1/_2$ and S = $^3/_2$ spin ground states.[17]

Table 2. Comparison of experimental and optimized structural metrics for [$Fe^{III}X(L^{ISQ})_2$] with S = $^3/_2$ and S = $^1/_2$ ground states.[a]

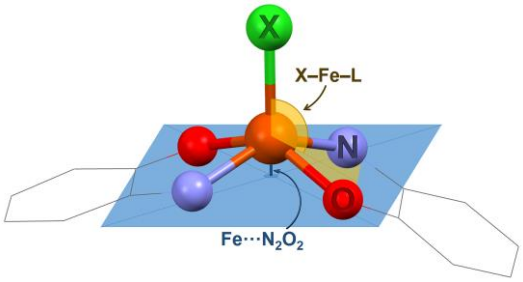

S = $^3/_2$	F	Cl		Br		I	N_3	NCS	
	calcd	calcd	exptl [c]	calcd	exptl [b]	calcd	calcd	calcd	exptl [b]
Fe–X	1.811	2.213	2.2203(7)	2.356	2.3685(5)	2.557	1.919	1.884	1.951(4)
Fe–O_{av}	2.000	1.992	1.963(1)	1.991	1.959(2)	1.984	1.997	1.994	1.943(4)
Fe–N_{av}	2.048	2.048	2.042(2)	2.046	2.045(2)	2.040	2.032	2.052	2.008(4)
Fe···O_2N_2[d]	0.69	0.67		0.66	0.62	0.63	0.61	0.66	0.54
X–Fe–L[e]	116.2	115.5		115.1	113.7	114.0	113.2	115.1	110.7

S = ½	F	Cl	Br		I		N_3		NCS
	calcd	calcd	calcd	exptl [b]	calcd	exptl [b]	calcd	exptl [b]	calcd
Fe–X	1.800	2.211	2.353	2.3665(9)	2.549	2.5910(3)	1.938	1.958(1)	1.849
Fe–O_{av}	1.914	1.908	1.907	1.873(3)	1.903	1.883(1)	1.931	1.8761(8)	1.922
Fe–N_{av}	1.902	1.897	1.897	1.892(4)	1.895	1.895(1)	1.906	1.883(1)	1.902
Fe···O_2N_2[d]	0.49	0.45	0.44	0.38	0.41	0.37	0.41	0.37	0.46
X–Fe–L[e]	109.7	108.4	107.7	105.5	106.7	105.2	106.2	105.1	108.6

[a] From BP86/def2-TZVPP calculations; distances in angstrom; angles in degrees; [b] Data taken from ref. [18]; [c] Data taken from ref. [17]; [d] Distance of Fe above the O_2N_2 plane; [e] Dihedral angle between Fe–X and {FeON} mean plane.

The key difference associated with the change of spin state is the shortening of the Fe–O and Fe–N bonds as the Fe ion moves closer to the O_2N_2 equatorial plane (0.41 – 0.49 Å). The pyramidalization

is larger for the $S = {}^3/_2$ species with the Fe ion residing 0.61 – 0.69 Å above the equatorial plane (Table 2). This structural feature is driven by the size of the halide ligand. The short bond distance required for a compact F^- ligand necessitates a greater pyramidalization about Fe to alleviate interligand repulsion with the equatorial *O*,*N*-chelates. In contrast, complexes with larger halides such as I^-, where the apical ligand is 0.7 – 0.8 Å further away from the Fe center, the interligand repulsion is less significant.

The $S = {}^1/_2$ ground state for $[Fe(N_3)(L^{ISQ})_2]$ is unexpected given it has hard donor apical ligand, and likely due to packing effects in the solid state. There are multiple intermolecular interactions between the azido ligand and hydrogen atoms of neighboring molecules in the crystal lattice may feasibly lead to a canting of the azido ligand of 110.5(1)°.[17] In contrast the isothiocyanato ligand in $[Fe(NCS)(L^{ISQ})_2]$ is near linear at 172.7(4)°. Given these features are reproduced in the gas phase optimized structures, we suggest that a particular resonance form leads to the tilting of the azido ligand, which in turn lowers the intraligand repulsion to favor the spin-doublet ground state.

The ground state electronic structures were computed using the broken symmetry (BS) DFT method on the two optimized geometries for each complex. A BS(5,2) calculation was used for the $M_S \approx S = {}^3/_2$ state and a BS(3,2) for the $M_S = S = {}^1/_2$ state, where the "5" and "3" define the number of unpaired electrons on the Fe(III) center. As these are transition metal complexes, a hybrid functional was employed. Previous DFT-based studies of square pyramidal Fe complexes with radical ligands had used the B3LYP functional with its 20% Hartree-Fock exchange (HFX) providing excellent results, especially with calculated spectroscopic observables.[10,11,16,19-21,28,29] For this series, however, B3LYP consistently favored the high-spin state over the intermediate-spin state when comparing their total energies. It well known the hybrid functional favor a high-spin configuration, and this increases with increasing exact HFX.[30] At the other end of the scale, generalized gradient approximation (GGA) functionals such as BP86 sans HFX favor the low-spin states due to rampant delocalization of spin density.[31] Bespoke computational investigations of benchmark iron spin-crossover compounds have proposed the optimal HFX resides between 10 – 17% for Fe(II) and Fe(III) species.[32] In order to determine the most appropriate level of HFX for the present study, calculations were carried out using

the B3LYP functional with the HFX set at 0%, 5%, 10% and 15%. It was revealed that B3LYP with 15% HFX – Reiher's B3LYP* functional – consistently gave the correct spin state energies across the series.[33,34] Several other theoretical studies of spin-crossover phenomena in iron compounds noted the standout performance of the B3LYP* functional.[35]

For the compounds where X = F, Cl and NCS, the $S = {}^3/_2$ state is more stable than the $S = {}^1/_2$ (Table 3). Only [FeCl(L^{ISQ})$_2$] gave an energy difference outside the accepted 3 – 5 kcal mol^{-1} resolution for DFT, though a <1 kcal mol^{-1} difference, equivalent to 500 K, is in the right temperature range for the observed spin transition. For X = Br, I and N_3, the spin-doublet is 2 – 3 kcal mol^{-1} more favorable than the spin-quartet, as seen experimentally.[17] For [FeBr(L^{ISQ})$_2$], where both the $S = {}^3/_2$ and $S = {}^1/_2$ species have been isolated and structurally characterized, magnetometric and Mössbauer measurements determined the onset of the spin-transition at 140 K. At reaching room temperature, the spin-quartet constituted 81.5% of the sample, and therefore the calculated value of 2 kcal mol^{-1} (ca. 1000 K) is an excellent estimate considering solid state effects have been ignored.

Table 3. Comparative energies (ΔE), exchange coupling constants (J), and Mulliken spin populations (ρ) for [FeX(L^{ISQ})$_2$].[a]

	S[b]	ρ_{Fe}	ρ_X	ρ_L[c]	ΔE[d]	J[e]
F	$^3/_2$	4.10	0.19	–1.30		–346
	$^1/_2$	2.46	0.17	–1.62	+0.3	–945
Cl	$^3/_2$	4.02	0.21	–1.22		–408
	$^1/_2$	2.56	0.20	–1.76	+5.2	+122
Br	$^3/_2$	4.00	0.21	–1.20		–424
	$^1/_2$	2.32	0.16	–1.48	–2.0	–1078
I	$^3/_2$	3.93	0.26	–1.18		–446
	$^1/_2$	2.32	0.17	–1.40	–2.6	–1127
N_3	$^3/_2$	4.03	0.24	–1.27		–466
	$^1/_2$	2.43	0.19	–1.62	–3.3	–1075
NCS	$^3/_2$	4.06	0.23	–1.30		–390
	$^1/_2$	2.43	0.22	–1.65	+0.7	–1017

[a] From B3LYP*/def-TZVPP calculations; [b] Total spin ground state; [c] Sum over both ligands; [d] Energy of $S = {}^1/_2$ relative to $S = {}^3/_2$, in kcal mol^{-1}; [e] Estimated exchange coupling constant, in cm^{-1}.

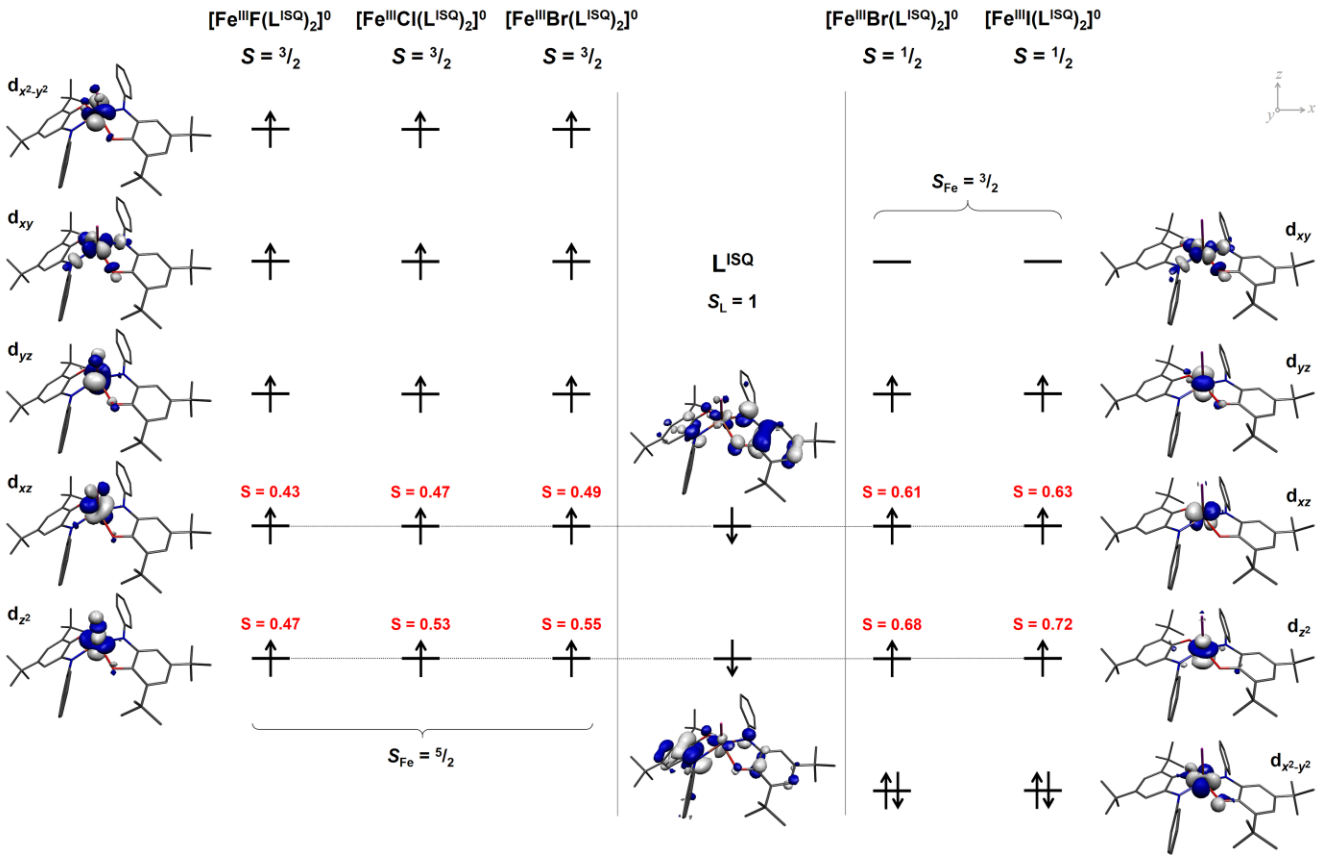

Figure 3. Qualitative MO scheme depicting the ordering of the frontier orbitals derived from BS(5,2) ground state calculations for $[FeX(L^{ISQ})_2]$ (X = F, Cl, Br), and BS(3,2) ground state calculations for $[FeX(L^{ISQ})_2]$ (X = Br, I) at the B3LYP*/def2-TZVPP level of theory. The five d-orbitals shown left are taken from $[FeF(L^{ISQ})_2]$ showing a high-spin Fe(III) ion; those on the right are from $[FeI(L^{ISQ})_2]$ and depict an intermediate-spin Fe(III) ion. The ligand-based β-spin orbitals are shown in the middle and antiferromagnetically couple to their symmetry-matched corresponding Fe-based α-spin orbital indicated by a dashed line. The spatial overlap (S) for each pair of corresponding magnetic orbitals is given.

The calculations show that the $S = {}^3/_2$ ground state for $[FeX(L^{ISQ})_2]$ (X = F, Cl, Br, I) comprises a high-spin Fe(III) $S_{Fe} = {}^5/_2$ central ion antiferromagnetically coupled to two ligand radicals (net $S_L = 1$). This solution is 10 – 13 kcal mol^{-1} more stable that the high-spin ($M_S = {}^7/_2$) solution where all three redox-active centers are ferromagnetically coupled. Five singly occupied molecular orbitals (SOMOs) are found in the α-spin (spin-up) manifold and two SOMOs are found in the β-spin (spin-down)

manifold (Figure 3). The α-spin SOMOs are all Fe-based with 77 – 93% d character whereas the β-spin SOMOs possess 85 – 90% ligand character, notably over both π-radical ligands (Figures S1 – S3). The strength of the coupling between the symmetry-matched pairs is estimated by the overlap integral (S) for these corresponding orbitals.[36] This parameter ranges S = 0 for uncoupled system to S = 1 for a standard, spin-pure solution. For the spin-quartet species, the overlap integrals are around S ≈ 0.5, and characteristic of a spin-singlet-coupled electron pair.[28] An estimate of the exchange coupling constant, *J*, yielded values of –346, –408 and –424 cm^{-1} for the F-, Cl- and Br-containing complexes, respectively (Table 3).[37] The *J*-value increases with increasing size of the halide because the longer Fe–X bond allows the π-radical ligands to shift closer to the Fe(III) ion improving orbital overlap.

The Mulliken spin population analysis for $[FeX(L^{ISQ})_2]$ (X = F, Cl, Br, I) calculated for an $S = {}^3/_2$ ground state shows ~4 spins on the Fe center (Table 3). This is less than the expected value for an $S_{Fe} = {}^5/_2$ ion because of covalent bonding to the apical halides and pseudo-halides which carry ca. 0.20 spins. The remaining spin is located on the *O*- and *N*-donor atoms in the equatorial plane through the σ-bonds, as seen in the spin density plot for $[FeBr(L^{ISQ})_2]$ displayed in Figure 4a. In addition to a small quantity of α-spin, each *O*,*N*-chelate carries –0.59 to –0.65 spins in their π MOs commensurate with a *o*-iminobenzosemiquinonato(1–) ligand radical. The spin density distribution varies with the nature of the apical ligand, with more localized spin distribution for the F^- and N_3^- hard donors, whereas the softer Br^- and I^- ligands increase covalency.

Optimization of each member of the series for an $S = {}^1/_2$ ground state resulted in a shift of the Fe–X unit toward the O_2N_2 equatorial plane (vide supra). This produces a stronger σ-antibonding interaction leading to destabilization of the d_{xy} orbital relative to the other d orbitals, leaving the non-bonding $d_{x^2-y^2}$ orbital doubly-occupied, and the d_{xz}, d_{yz} and d_{z^2} orbitals singly-occupied – the hallmark of an intermediate-spin Fe(III) ion. The qualitative MO scheme for the BS(3,2) solution presented in Figure 3 exhibits these exact features. In each calculation, the BS solution ($M_S = {}^1/_2$) was around 20 kcal mol^{-1} more stable than the high-spin state ($M_S = {}^5/_2$), except for $[FeCl(L^{ISQ})_2]$, where the high-spin state was preferred by 2.5 kcal mol^{-1}. Attempts to produce a low-spin Fe(III) $S_{Fe} = {}^1/_2$ state from a BS(2,1)

calculation instead converged to the BS(3,2) solution. Two SOMOs with ~85% ligand character are identified in the β-spin manifold, and these are antiferromagnetically coupled to the corresponding Fe SOMOs of matching symmetry. The shorter Fe–O and Fe–N distances in the S = $^1/_2$-optimized structures results in greater overlap of these pairs of magnetic orbitals as evidenced by the larger overlap integrals of S = 0.6 – 0.7. The calculated J-values are more than double those in the spin-quartet species at *ca*. –1000 cm^{-1}, except for [FeCl(L^{ISQ})$_2$], where the high-spin (M_S = $^5/_2$) solution is favored over the BS (M_S = $^1/_2$) one giving J = +122 cm^{-1} (Table 3). Interestingly, the d_{z^2} orbital is singly-occupied in both the S = $^3/_2$ and S = $^1/_2$ states, hence the negligible effect of the iron spin state on the Fe–X bond length (Table 2). The Mulliken spin population analysis shows ~2.4 spins are localized to the iron ion and the remaining α-spin distributed to the apical halide ligand (Figure 4b). The L^{ISQ} radical ligands each hold –0.7 to –0.9 spins, with the hard donors producing slightly more polarized equatorial bonds.

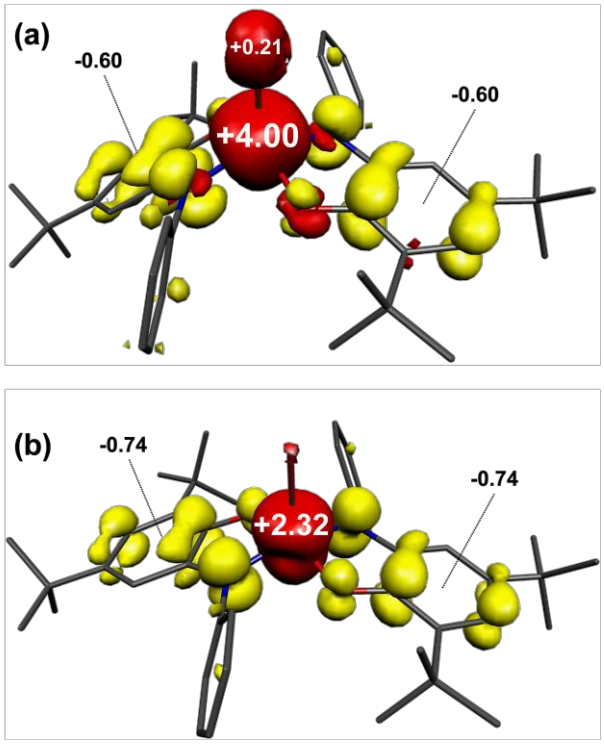

Figure 4. Comparison of the Mulliken spin density distribution in [FeBr(L^{ISQ})$_2$] for (a) an S = $^3/_2$ and (b) an S = $^1/_2$ ground state (red: α-spin; yellow: β-spin).

Within the present B3LYP* DFT methodology, it is possible to calculate Mössbauer parameters as a means to verify the calculated electronic structures for this [FeX(L^{ISQ})$_2$] series with both S = $^3/_2$ and S = $^1/_2$ spin ground states.[38] The calculated isomer shift (δ) and quadrupole splitting (ΔE_Q) for the iron ion are listed in Table 4, and compared with the experimental data obtained on powder samples at 80 K.[17,18] Overall the calculated parameters are in excellent agreement with the experiment. The calculated ΔE_Q shows a slightly greater deviation due to the difference between solid state and gas phase structures for the complexes, as well as the varying mixtures of S = $^3/_2$ and S = $^1/_2$ species for some of the complexes at 80 K. The greatest disparity is for [Fe(N_3)(L^{ISQ})$_2$], where at 80 K, the compound is exclusively S = $^1/_2$.[17] This difference is not a consequence of the geometry, as the optimized structure gives slightly better ΔE_Q than that calculated on the crystallographic coordinates where the only noticeable difference is the orientation of the apical ligand – 110.5° in the crystal structure; 117.4° in the optimized structure. As the isomer shift is less sensitive to these minor structural changes, it remains constant. Overall, the spin-quartet species with their high-spin Fe(III) ion have a larger isomer shift than the intermediate-spin Fe(III) ion in the spin-doublet species.[39]

Table 4. Comparison of calculated and experimental (in parentheses) Mössbauer parameters for [FeX(L^{ISQ})$_2$].[a]

	S [a]	δ / mm s^{-1} [c]		ΔE_Q / mm s^{-1} [c]	
F	$^3/_2$	0.49		–1.12	
Cl	$^3/_2$	0.42	(0.45)	1.08	(1.26)
Br	$^3/_2$	0.42	(0.47)	1.05	(1.22)
	$^1/_2$	0.27	(0.23)	2.10	(2.62)
I	$^1/_2$	0.25	(0.24)	2.18	(2.80)
N_3	$^1/_2$	0.29	(0.20)	1.80	(2.42)
		0.30[d]		1.67[d]	
NCS	$^3/_2$	0.43	(0.43)	1.28	(1.26)

[a] From B3LYP*/def2-TZVPP calculations; [b] Total spin ground state; [c] Experimental data taken from ref. [17]; [d] Calculated on the crystallographic coordinates.

Moreover, the high-spin Fe(III) ion has a significantly smaller quadrupole splitting consistent with its even electron distribution compared with the more anisotropic electron distribution for an intermediate-spin d^5 ion. As zero-field Mössbauer spectra are unable to reveal the sign of the quadrupole splitting, the calculations suggest a positive value for all except $[FeF(L^{ISQ})_2]$.

3. Electron transfer series. To investigate the effect of changing the ligand oxidation level, the electronic structures of the putative five-membered electron transfer series of $[FeF(L^{ISQ})_2]^z$ and $[FeI(L^{ISQ})_2]^z$ (z = 2+, 1+, 0, 1–, 2–) were calculated at the B3LYP* level of theory. These complexes were chosen as the charge-neutral members have pure $S = {}^3/_2$ and $S = {}^1/_2$ ground states, respectively. The process began with a gas phase optimization (BP86/def2-TZVPP) for each of the three iron spin state options: high-spin, ($S_{Fe} = {}^5/_2$), intermediate-spin ($S_{Fe} = {}^3/_2$) and low-spin ($S_{Fe} = {}^1/_2$), followed by a single-point calculation (B3LYP*/def2-TZVPP) to compare spin state energies. Both electron transfer series are related by one-electron redox events localized to the *O*,*N*-chelates with the iron center remaining +III (Eq. 1). Although these compounds have not been subject to an electrochemical investigation, related square pyramidal Fe(III) complexes with redox-active chelates do undergo one-electron redox reactions which are ligand-centered,[16,20] as exemplified by homoleptic complexes with group 10 metals.[7] ń

$$[Fe^{III}X(L^{IBQ})_2]^{2+} \underset{-e}{\overset{+e}{\rightleftharpoons}} [Fe^{III}X(L^{ISQ})(L^{IBQ})]^{1+} \underset{-e}{\overset{+e}{\rightleftharpoons}} [Fe^{III}X(L^{ISQ})_2]^{0} \underset{-e}{\overset{+e}{\rightleftharpoons}} [Fe^{III}X(L^{AP})(L^{ISQ})]^{1-} \underset{-e}{\overset{+e}{\rightleftharpoons}} [Fe^{III}X(L^{AP})_2]^{2-} \quad (1)$$

Oxidation of the charge neutral species with two radical $(L^{ISQ})^{1-}$ ligands gave dicationic complexes with two neutral $(L^{IBQ})^0$ ligands. On the other hand, reduction produced dianionic complexes with two dianionic $(L^{AP})^{2-}$ ligands. The charge states in between these limits, the monocationic and monoanionic members of the series, have one radical $(L^{ISQ})^{1-}$ paired with either a neutral $(L^{IBQ})^0$ or a dianionic $(L^{AP})^{2-}$ ligand (Eq. 1). These complexes exhibit class III mixed-valency (fully delocalized) with the oxidation level distributed over both ligands.[40] This is seen in the intraligand bond distances of the optimized structures being identical for both ligands (Tables S3 and S4). Similarly, the Mulliken spin

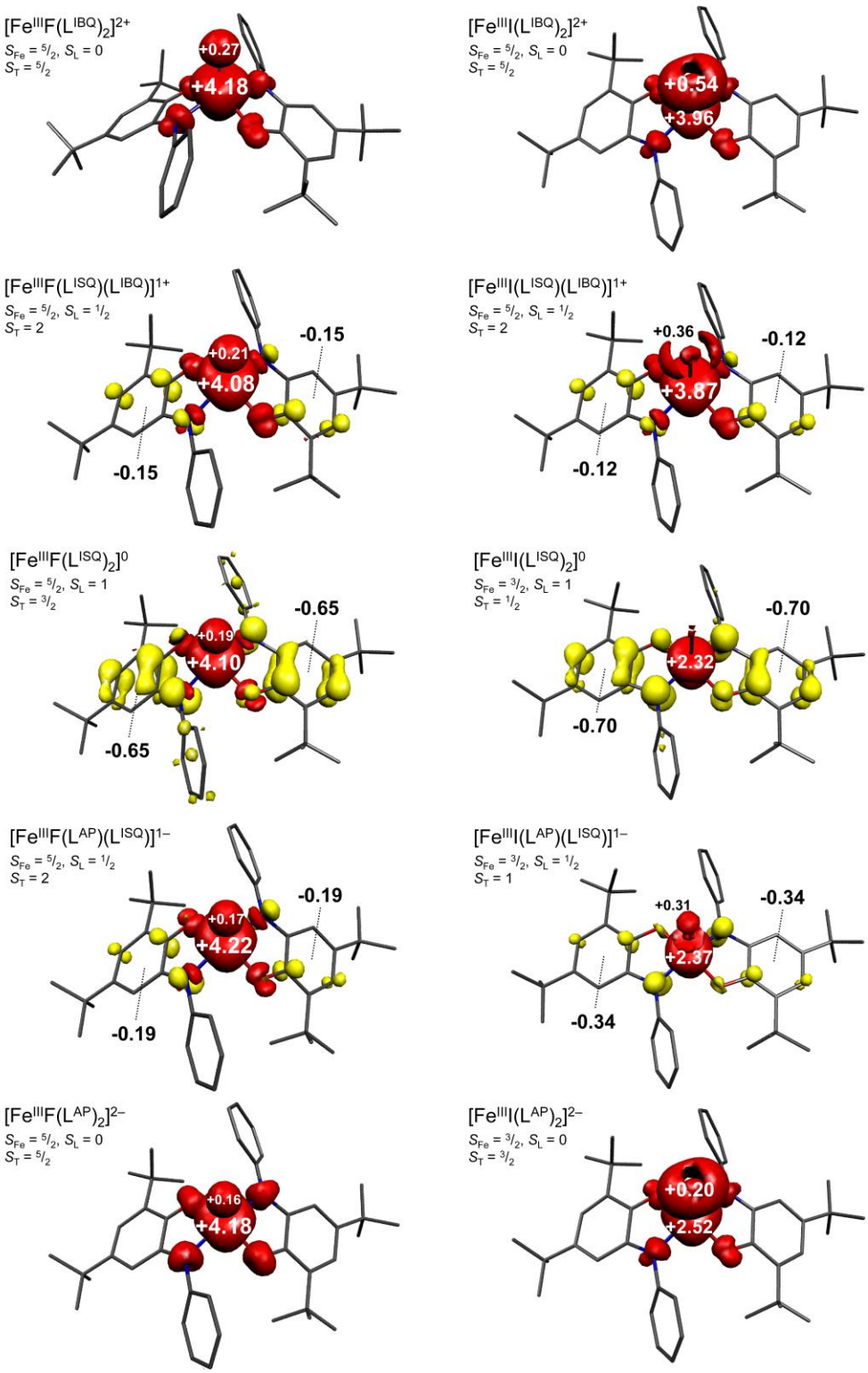

Figure 6. Mulliken spin density plots for each member of the $[FeF(L)_2]^z$ (left) and $[FeI(L)_2]^z$ (right; z = 2+, 1+, 0, 1–, 2–) electron transfer series (red: α-spin; yellow: β-spin). The Fe, L and total spin states are given.

analysis of the monocationic and monoanionc members of the series shows one unpaired electron (β-spin) equally distribution over the two *O*,*N*-chelates (Figure 6). The apical F^- ion as a hard donor ligand ensures the Fe(III) remains in the high-spin state throughout the electron transfer series (Table S5). This is expected for the cationic complexes where the ligand field strength diminishes with the removal of charge from the equatorial ligands when the $(L^{ISQ})^{1-}$ radicals are oxidized to the (L^{IBQ}) form (Scheme 1). Oxidation of the system results in a shortening of the Fe–F bond, and a shift of this unit further from the O_2N_2 equatorial plane, increasing the pyramidalization at iron (Table S3). Although the ligand field is strengthened upon reduction of the ligands to their dianionic form, when combined with an apical F^- ion, the high-spin Fe(III) state is favored. The reduced species have slightly shorter Fe–O bonds as the oxygen atom now bears a formal negative charge, whereas the Fe–N distances remain unchanged between the $(L^{ISQ})^{1-}$ and $(L^{AP})^{2-}$ levels. The Fe ion remains ~0.7 Å above the equatorial plane and the increased charge on the equatorial ligands leads to a lengthening of the Fe–F bond to counter interligand repulsion. This is shown in the Mulliken spin density distribution where the portion of α-spin delocalized to the fluoro ligand decreases for the reduced complexes (Figure 6). The low-spin Fe(III) state is the least favored configuration for all members of this series, at 14 – 18 kcal mol^{-1} higher in energy (Table S5).

For the $[FeI(L^{ISQ})_2]^z$ (z = 2+, 1+, 0, 1–, 2–) transfer series, the oxidized members also favor a high-spin Fe(III) S_{Fe} = $^5/_2$ central ion by 5.0 and 7.2 kcal mol^{-1} for the monocationic and dicationic complexes, respectively. The Mulliken spin population analysis sees ca. +3.9 spins on the Fe ion with a sizeable quotient deposited on the iodo ligand through its covalent bond (Figure 6). A change in spin state occurs with the charge-neutral species, where an intermediate-spin Fe(III) S_{Fe} = $^3/_2$ ion is favored, albeit marginally for the monoanionic and dianionic members of the series when comparing total energies (Table S6). The change to an intermediate-spin Fe(III) ion sees +2.32, +2.37 and +2.52 spins localized at the Fe center in the neutral, monoanionic and dianionic members, respectively. This value is less than the ideal 3 spins for an intermediate-spin ion due to covalent bonding, which leads to α-spin deposited on all first coordination sphere donor atoms. The larger value for the dianionic complex comes about from the elongation of the Fe–I bond by ca. 0.2 Å to alleviate the interligand

repulsion due to the extra negative charge from the two dianionic ligands in the equatorial plane. As mentioned above, the ligand field strength is insufficient to stabilize a low-spin Fe(III) $S_{Fe} = {}^1/_2$ central ion.

Conclusions

This study completes the theoretical examination of square pyramidal Fe(III) complexes with two redox-active bidentate ligands. Unlike for the *N*,*N*-, *N*,*S*- and *S*,*S*-chelates, these *O*,*N*-chelates in combination with an apical halide or pseudo-halide introduce an experimentally observable $S = {}^3/_2 \rightarrow S = {}^5/_2$ spin transition at the Fe(III) central. Using the available crystallographic and spectroscopic data to calibrate the DFT method, it is shown that reliable spin state energies are calculated using the B3LYP* functional with 15% HFX. This computational protocol was used to examine the potential redox chemistry of these compounds, with the five-membered electron transfer series were related by successive one-electron transfer steps localized to the chelating ligands. With a hard apical donor, the ferric ion is preferably high-spin irrespective to the equatorial ligand oxidation level. In complexes with a large apical halide ligand that is further from the Fe ion, the diminished interligand repulsion enables the equatorial ligands to bind more tightly and switch the iron center to an intermediate-spin configuration. The potential of Fe(II) and Fe(III) ions to adopt three different spin states modulated by the ligand field is an important consideration in the application of such species in catalytic reactions. Increasingly theoretical methods are used to qualify a mechanistic pathway by defining plausible active species and intermediates, and an experimentally verified computational method is an invaluable asset toward the exploiting the redox interplay between Earth abundant transition metal and radical ligands.

Experimental Section

Theoretical calculations. All calculations in this work were performed with the electronic structure program ORCA.[41] Geometry optimizations and numerical frequencies were carried out using the

BP86 functional.[42] All-electron Gaussian basis sets were those developed by the Ahlrich's group.[43] Triple-ζ-quality basis sets with two sets of polarization functions (def2-TZVPP) were used for all atoms with enhanced integration accuracy on iron of 10 and the halide/pseudo-halide of 7.[44] A scalar relativistic correction was applied using the zeroth-order regular approximation (ZORA) method[45] as implemented by van Wüllen.[46] Auxiliary basis sets used to expand the electron density in the resolution-of-the-identity (RI) approach were chosen, where applicable, to match the orbital basis.[47] A spin-unrestricted formulism was applied to all species. The self-consistent field (SCF) calculations were tightly converged (1×10^{-8} E_h in energy, 1×10^{-7} E_h in the density change, and 1×10^{-7} in the maximum element of the DIIS[48] error vector). The geometry search for all complexes was carried out in redundant internal coordinates without imposing geometry constraints. Single-point DFT calculations on geometry optimized coordinates using the B3LYP* hybrid functional,[33] which is a modified variant of the standard B3LYP functional[49] with 15% Hartree-Fock exchange. The RIJCOSX algorithm was used to speed the calculation of Hartree–Fock exchange.[50]

The broken symmetry (BS) approach is used for the computational results of all compounds.[51] The following notation is adopted for a given system divided into two fragments: The notation BS(*m*,*n*) refers then to a broken symmetry state with *m* unpaired α-spin electrons essentially on fragment 1 and *n* unpaired β-spin electrons localized on fragment 2. In this notation the standard high-spin (HS), open-shell solution is written as BS(*m*+*n*,0). The BS(*m*,*n*) notation refers to the initial guess to the wavefunction. The variational process does, however, have the freedom to converge to a solution of the form BS(*m*−*n*,0) in which effectively the *n* β-spin electrons pair up with $n < m$ α-spin electrons on the partner fragment. Such a solution is then a standard $M_S \approx (m-n)/2$ spin-unrestricted Kohn-Sham solution. The nature of the solution is investigated from the corresponding orbital transformation[36] which, from the corresponding orbital overlaps, displays whether the system should be described as a spin-coupled or a closed-shell solution.

The exchange coupling constants *J* were obtained from broken symmetry solution using Eq. 2,[37] and assuming the spin-Hamiltonian Eq. 3 is valid,

$$J = \frac{E_{HS} - E_{BS}}{\langle \hat{S}^2 \rangle_{HS} - \langle \hat{S}^2 \rangle_{BS}} \quad (2)$$

$$\hat{H} = -2J\hat{S}_A \cdot \hat{S}_B \quad (3)$$

where E_{BS} is the energy of the broken symmetry solution, E_{HS} is the energy of the high spin state, $\langle \hat{S}^2 \rangle_{HS}$ is the expectation value of $\hat{S}^2$ operator for the high spin state, $\langle \hat{S}^2 \rangle_{BS}$ is the expectation value of $\hat{S}^2$ operator for the broken symmetry solution, and $\langle \hat{S}^2 \rangle_{HS}$ is the expectation value of $\hat{S}_A^2$ and $\hat{S}_B^2$ are local spin operators. Canonical and corresponding orbitals,[36] as well as spin density plots were generated with the program Molekel.[52] Nonrelativistic single-point calculations on the optimized geometry were carried out to predict Mössbauer spectral parameters (isomer shifts and quadrupole splittings). These calculations employed the CP(PPP) basis set for iron.[53] The Mössbauer isomer shifts were calculated from the computed electron densities at the iron centers as previously described.[38]

Acknowledgments

We thank the University of Glasgow for providing access to computational resources and financial support.

Conflict of Interest

The authors declare no conflict of interest.

Keywords: density functional theory • electronic structure • iron complexes • ligand radicals • spin transition

References

[1] a) *Catalytic Asymmetric Synthesis*, 2nd ed., Wiley-VCH, New York, **2004**; b) G. W. Parshall, S. D. Ittel, *Homogeneous Catalystis: The Applications and Chemistry of Catalysis by Soluble Transition Metal Complexes*, 2nd ed., Wiley, New York, **1992**.

[2] R. Arevalo, P. J. Chirik, *J. Am. Chem. Soc.* **2019**, *141*, 9106.

[3] a) P. J. Chirik, R. Morris, *Acc. Chem. Res.* **2015**, *48*, 2495; b) J. V. Obligacion, P. J. Chirik, *Nat. Rev. Chem.* **2018**, *2*, 15; c) E. P. Beaumier, A. J. Pearce, X. Y. See, I. A. Tonks, *Nat. Rev. Chem.* **2019**, *3*, 15.

[4] P. J. Chirik, K. Wieghardt, *Science* **2010**, *327*, 794.

[5] P. J. Chirik, *Acc. Chem. Res.* **2015**, *48*, 1687.

[6] J. Stubbe, W. A. van der Donk, *Chem. Rev.* **1998**, *98*, 705.

[7] P. Chaudhuri, C. N. Verani, E. Bill, E. Bothe, T. Weyhermüller, K. Wieghardt, *J. Am. Chem. Soc.* **2001**, *123*, 2213.

[8] P. Chaudhuri, K. Wieghardt, *Prog. Inorg. Chem.* **2001**, *50*, 151.

[9] S. Sproules, *Prog. Inorg. Chem.* **2014**, *58*, 1.

[10] S. Sproules, K. Wieghardt, *Coord. Chem. Rev.* **2011**, *255*, 837.

[11] a) K. Ray, T. Petrenko, K. Wieghardt, F. Neese, *Dalton Trans.* **2007**, 1552; b) S. Sproules, K. Wieghardt, *Coord. Chem. Rev.* **2010**, *254*, 1358.

[12] a) D. Sellmann, S. Emig, F. W. Heinemann, *Angew. Chem. Int. Ed.* **1997**, *36*, 1734; b) D. Sellmann, S. Emig, F. W. Heinemann, *Angew. Chem. Int. Ed.* **1997**, *36*, 1201.

[13] P. Ghosh, E. Bill, T. Weyhermüller, K. Wieghardt, *J. Am. Chem. Soc.* **2003**, *125*, 3967.

[14] S. Sproules, *Angew. Chem. Int. Ed.* **2019**, *58*, 10043.

[15] a) S. Blanchard, E. Bill, T. Weyhermüller, K. Wieghardt, *Inorg. Chem.* **2004**, *43*, 2324; b) K. Chłopek, E. Bill, T. Weyhermüller, K. Wieghardt, *Inorg. Chem.* **2005**, *44*, 7087; c) P. Ghosh, A. Begum, E. Bill, T. Weyhermüller, K. Wieghardt, *Inorg. Chem.* **2003**, *42*, 3208; d) C. Mukherjee, T. Weyhermüller, E. Bothe, P. Chaudhuri, *Inorg. Chem.* **2008**, *47*, 11620; e) S. R. Presow, M. Ghosh, E. Bill, T. Weyhermüller, K. Wieghardt, *Polyhedron* **2011**, *374*, 226; f) A. M. Whalen, S.

Bhattacharya, C. G. Pierpont, *Inorg. Chem.* **1994**, *33*, 347; g) B. Xu, A. Ma, T. Jia, Z. Hao, W. Gao, Y. Mu, *Dalton Trans.* **2016**, *45*, 17966.

[16] K. Chłopek, N. Muresan, F. Neese, K. Wieghardt, *Chem. Eur. J.* **2007**, *13*, 8390.

[17] H. Chun, E. Bill, T. Weyhermüller, K. Wieghardt, *Inorg. Chem.* **2003**, *42*, 5612.

[18] H. Chun, T. Weyhermüller, E. Bill, K. Wieghardt, *Angew. Chem. Int. Ed.* **2001**, *40*, 2489.

[19] P. Ghosh, E. Bill, T. Weyhermüller, F. Neese, K. Wieghardt, *J. Am. Chem. Soc.* **2003**, *125*, 1293.

[20] A. K. Patra, E. Bill, E. Bothe, K. Chłopek, F. Neese, T. Weyhermüller, K. Stobie, M. D. Ward, J. A. McCleverty, K. Wieghardt, *Inorg. Chem.* **2006**, *45*, 7877.

[21] a) T. Petrenko, K. Ray, K. Wieghardt, F. Neese, *J. Am. Chem. Soc.* **2006**, *128*, 4422; b) K. Ray, A. Begum, T. Weyhermüller, S. Piligkos, J. van Slageren, F. Neese, K. Wieghardt, *J. Am. Chem. Soc.* **2005**, *127*, 4403; c) N. Roy, S. Sproules, E. Bill, T. Weyhermüller, K. Wieghardt, *Inorg. Chem.* **2008**, *47*, 10911; d) M. D. Symes, Makara J. Sci. **2016**, *20*, 155; e) N. Roy, S. Sproules, T. Weyhermüller, K. Wieghardt, *Inorg. Chem.* **2009**, *48*, 3783; f) P. Surawatanawong, S. Sproules, F. Neese, K. Wieghardt, *Inorg. Chem.* **2011**, *50*, 12064.

[22] K. Ray, T. Weyhermüller, F. Neese, K. Wieghardt, *Inorg. Chem.* **2005**, *44*, 5345.

[23] a) B. Chakraborty, S. Bhunya, A. Paul, T. K. Paine, *Inorg. Chem.* **2014**, *53*, 4899; b) M. M. Bittner, S. V. Lindeman, A. T. Fiedler, *J. Am. Chem. Soc.* **2012**, *134*, 5460; c) G. C. Paul, S. Banerjee, C. Mukherjee, *Inorg. Chem.* **2017**, *56*, 729.

[24] a) A. L. Smith, L. E. Clapp, K. I. Hardcastle, J. D. Soper, *Polyhedron* **2010**, *29*, 164; b) A. L. Smith, K. I. Hardcastle, J. D. Soper, *J. Am. Chem. Soc.* **2010**, *132*, 14358.

[25] C. A. Lippert, K. I. Hardcastle, J. D. Soper, *Inorg. Chem.* **2011**, *50*, 9864.

[26] H. Chun, E. Bill, E. Bothe, T. Weyhermüller, K. Wieghardt, *Inorg. Chem.* **2002**, *41*, 5091.

[27] A. N. Erickson, S. N. Brown, *Dalton Trans.* **2018**, *47*, 15583.

[28] V. Bachler, O. Gottfried, F. Neese, K. Wieghardt, *Inorg. Chem.* **2002**, *41*, 4179.

[29] a) P. Banerjee, S. Sproules, T. Weyhermüller, S. DeBeer George, K. Wieghardt, *Inorg. Chem.* **2009**, *48*, 5829; b) E. Bill, E. Bothe, P. Chaudhuri, K. Chłopek, D. Herebian, S. Kokatam, K. Ray,

T. Weyhermüller, F. Neese, K. Wieghardt, *Chem. Eur. J.* **2005**, *11*, 204; c) K. Chłopek, E. Bothe, F. Neese, T. Weyhermüller, K. Wieghardt, *Inorg. Chem.* **2006**, *45*, 6298; d) D. Herebian, K. Wieghardt, F. Neese, *J. Am. Chem. Soc.* **2005**, *125*, 10997; e) R. R. Kapre, K. Ray, I. Sylvestre, T. Weyhermüller, S. DeBeer George, F. Neese, K. Wieghardt, *Inorg. Chem.* **2006**, *45*, 3499; f) S. Kokatam, K. Ray, J. Pap, E. Bill, W. E. Geiger, R. J. LeSuer, P. H. Rieger, T. Weyhermüller, F. Neese, K. Wieghardt, *Inorg. Chem.* **2007**, *46*, 1100; g) M. Li, D. Bonnet, E. Bill, F. Neese, T. Weyhermüller, N. Blum, D. Sellmann, K. Wieghardt, *Inorg. Chem.* **2002**, *41*, 3444; h) C. Milsmann, S. Sproules, E. Bill, T. Weyhermüller, S. DeBeer George, K. Wieghardt, *Chem. Eur. J.* **2010**, *16*, 3628; i) K. Ray, E. Bill, T. Weyhermüller, K. Wieghardt, *J. Am. Chem. Soc.* **2005**, *127*, 5641; j) K. Ray, S. DeBeer George, E. I. Solomon, K. Wieghardt, F. Neese, *Chem. Eur. J.* **2007**, *13*, 2783; k) N. Roy, S. Sproules, E. Bothe, T. Weyhermüller, K. Wieghardt, *Eur. J. Inorg. Chem.* **2009**, 2655; l) S. Sproules, P. Banerjee, T. Weyhermüller, Y. Yan, J. P. Donahue, K. Wieghardt, *Inorg. Chem.* **2011**, *50*, 7106; m) S. Sproules, F. L. Benedito, E. Bill, T. Weyhermüller, S. DeBeer George, K. Wieghardt, *Inorg. Chem.* **2009**, *48*, 10926; n) S. Sproules, T. Weyhermüller, R. Goddard, K. Wieghardt, *Inorg. Chem.* **2011**, *50*, 12623.

[30] M. Swart, *Int. J. Quantum Chem.* **2013**, *113*, 2.

[31] D. A. Pantazis, *Inorganics* **2019**, *7*, 57.

[32] O. S. Siig, K. P. Kepp, *J. Phys. Chem. A* **2018**, *122*, 4208.

[33] M. Reiher, O. Salomon, B. A. Hess, *Theor. Chem. Acc.* **2001**, *107*, 48.

[34] O. Salomon, M. Reiher, B. A. Hess, *J. Chem. Phys.* **2002**, *117*, 4729.

[35] a) J. Cirera, M. Via-Nadal, E. Ruiz, *Inorg. Chem.* **2018**, *57*, 14097; b) Q. M. Phung, A. Domingo, K. Pierloot, *Chem. Eur. J.* **2018**, *24*, 5183; c) K. P. Kepp, *Inorg. Chem.* **2016**, *55*, 2717.

[36] F. Neese, *J. Phys. Chem. Solids* **2004**, *65*, 781.

[37] a) K. Yamaguchi, Y. Takahara, T. Fueno, in *Applied Quantum Chemistry* (Ed.: V. H. Smith), Reidel, Dordrecht, The Netherlands, **1986**, p. p. 155; b) T. Soda, Y. Kitagawa, T. Onishi, Y. Takano, Y. Shigetu, H. Nagao, Y. Yoshioka, K. Yamaguchi, *Chem. Phys. Lett.* **2000**, *319*, 223-230.

[38] M. Pápai, G. Vankó, *J. Chem. Theory Comput.* **2013**, *9*, 5004.

[39] P. Gütlich, E. Bill, A. X. Trautwein, *Mössbauer Spectroscopy and Transition Metal Chemistry*, Springer-Verlag, Berlin Heidelberg, **2011**.

[40] C. C. Lu, E. Bill, T. Weyhermüller, E. Bothe, K. Wieghardt, *J. Am. Chem. Soc.* **2008**, *130*, 3181.

[41] F. Neese, *WIREs Comput. Molec. Sci.* **2012**, *2*, 73.

[42] A. D. Becke, *Phys. Rev. A* **1988**, *38*, 3098; b) J. P. Perdew, *Phys. Rev. B* **1986**, *33*, 8822.

[43] a) R. Ahlrichs, K. May, *Phys. Chem. Chem. Phys.* **2000**, *2*, 943; b) F. Weigend, R. Ahlrichs, *Phys. Chem. Chem. Phys.* **2005**, *7*, 3297; c) F. Weigend, *Phys. Chem. Chem. Phys.* **2006**, *8*, 1057.

[44] D. A. Pantazis, X.-Y. Chen, C. R. Landis, F. Neese, *J. Chem. Theory Comput.* **2008**, *4*, 908.

[45] a) E. van Lenthe, J. G. Snijders, E. J. Baerends, *J. Chem. Phys.* **1996**, *105*, 6505; b) E. van Lenthe, A. van der Avoird, P. E. S. Wormer, *J. Chem. Phys.* **1998**, *108*, 4783; c) J. H. van Lenthe, S. Faas, J. G. Snijders, *Chem. Phys. Lett.* **2000**, *328*, 107.

[46] C. J. van Wüllen, *J. Chem. Phys.* **1998**, *109*, 392.

[47] a) K. Eickhorn, O. Treutler, H. Ohm, M. Haser, R. Ahlrichs, *Chem. Phys. Lett.* **1995**, *242*, 652; b) K. Eickhorn, F. Weigend, O. Treutler, R. Ahlrichs, *Theor. Chem. Acc.* **1997**, *97*, 119.

[48] a) P. Pulay, *Chem. Phys. Lett.* **1980**, *73*, 393; b) P. Pulay, *J. Comput. Chem.* **1982**, *3*, 556.

[49] a) A. D. Becke, *J. Chem. Phys.* **1993**, *98*, 5648; b) C. T. Lee, W. T. Yang, R. G. Parr, *Phys. Rev. B* **1988**, *37*, 785.

[50] F. Neese, F. Wennmohs, A. Hansen, U. Becker, *Chem. Phys.* **2009**, *356*, 98.

[51] a) L. Noodleman, *J. Chem. Phys.* **1981**, *74*, 5737; b) L. Noodleman, D. A. Case, A. Aizman, *J. Am. Chem. Soc.* **1988**, *110*, 1001; c) L. Noodleman, E. R. Davidson, *Chem. Phys.* **1986**, *109*, 131; d) L. Noodleman, J. G. Norman, J. H. Osborne, A. Aizman, D. A. Case, *J. Am. Chem. Soc.* **1985**, *107*, 3418; e) L. Noodleman, C. Y. Peng, D. A. Case, J. M. Monesca, *Coord. Chem. Rev.* **1995**, *144*, 199.

[52] *Molekel*, Advanced Interactive 3D-Graphics for Molecular Sciences, Swiss National Supercomputing Center. https://ugovaretto.github.io/molekel/

[53] F. Neese, *Inorg. Chim. Acta* **2002**, *337*, 181.

TOC entry

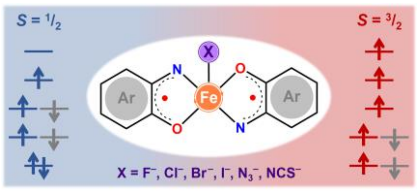

Ground state electronic structures for the square pyramidal complexes $[Fe^{III}X(L^{ISQ})_2]^0$ (X = F^-, Cl^-, Br^-, I^-, N_3^-, NCS^-) with two *o*-iminobenzosemiquinonato π-radical ligands have been calculated using DFT. Using the B3LYP* functional with 15% Hartree-Fock exchange, the iron spin state, which is dependent on the nature of the X ligand, was accurately reproduced and highlight the importance of having an experimentally validated computational protocol.